

# How predictable is the northern hemisphere summer upper-tropospheric circulation?

June-Yi Lee · Bin Wang · Q. Ding · K.-J. Ha ·  
J.-B. Ahn · A. Kumar · B. Stern · O. Alves

Received: 15 March 2010 / Accepted: 10 September 2010 / Published online: 1 October 2010  
© Springer-Verlag 2010

**Abstract** The retrospective forecast skill of three coupled climate models (NCEP CFS, GFDL CM2.1, and CAWCR POAMA 1.5) and their multi-model ensemble (MME) is evaluated, focusing on the Northern Hemisphere (NH) summer upper-tropospheric circulation along with surface temperature and precipitation for the 25-year period of 1981–2005. The seasonal prediction skill for the NH 200-hPa geopotential height basically comes from the coupled models' ability in predicting the first two empirical orthogonal function (EOF) modes of interannual variability, because the models cannot replicate the residual higher modes. The first two leading EOF modes

of the summer 200-hPa circulation account for about 84% (35.4%) of the total variability over the NH tropics (extratropics) and offer a hint of realizable potential predictability. The MME is able to predict both spatial and temporal characteristics of the first EOF mode (EOF1) even at a 5-month lead (January initial condition) with a pattern correlation coefficient (PCC) skill of 0.96 and a temporal correlation coefficient (TCC) skill of 0.62. This long-lead predictability of the EOF1 comes mainly from the prolonged impacts of El Niño-Southern Oscillation (ENSO) as the EOF1 tends to occur during the summer after the mature phase of ENSO. The second EOF mode (EOF2), on the other hand, is related to the developing ENSO and also the interdecadal variability of the sea surface temperature over the North Pacific and North Atlantic Ocean. The MME also captures the EOF2 at a 5-month lead with a PCC skill of 0.87 and a TCC skill of 0.67, but these skills are mainly obtained from the zonally symmetric component of the EOF2, not the prominent wavelike structure, the so-called circumglobal teleconnection (CGT) pattern. In both observation and the 1-month lead MME prediction, the first two leading modes are accompanied by significant rainfall and surface air temperature anomalies in the continental regions of the NH extratropics. The MME's success in predicting the EOF1 (EOF2) is likely to lead to a better prediction of JJA precipitation anomalies over East Asia and the North Pacific (central and southern Europe and western North America).

---

J.-Y. Lee (✉) · B. Wang  
International Pacific Research Center,  
University of Hawaii/IPRC, POST Bldg, Room 409A,  
1680 East-West Road, Honolulu, HI 96822, USA  
e-mail: jyilee@soest.hawaii.edu

Q. Ding  
Department of Earth and Space Sciences and Quaternary  
Research Center, University of Washington, Seattle,  
Washington 98195, USA

K.-J. Ha · J.-B. Ahn  
Division of Earth Environmental System,  
Pusan National University, Busan, Korea

A. Kumar  
NCEP/CPC, Camp Springs, MD, USA

B. Stern  
NOAA/GFDL, Princeton University, Princeton, NJ, USA

O. Alves  
Centre for Australia Weather and Climate Research (CAWCR),  
Bureau of Meteorology, Melbourne, VIC, Australia

**Keywords** Seasonal climate coupled model prediction · Realizable potential predictability · Realized prediction skill · Predictable mode · Summer upper-tropospheric circulation · Multi-model ensemble prediction · Tropical-extratropical teleconnection · El Niño-Southern oscillation

## 1 Introduction

Using 14 climate prediction models, Wang et al. (2009) demonstrated that the 1-month lead seasonal multi-model ensemble (MME) prediction is less skillful in predicting summertime atmospheric variability in the Northern Hemisphere (NH) extratropics compared to its winter counterpart. Nonetheless, the MME prediction has useful forecast skill over some specific geographical locations including East Asia and eastern North America, suggesting that “predictable patterns” may exist in the NH extratropics during summer and may be associated with the tropical-extratropical teleconnection patterns.

The teleconnection patterns of boreal summer NH atmospheric circulation, from either a regional or global point of view, have received much attention in recent years, mainly focusing on the linkages with the Asian summer monsoon variability concurrent with ENSO (Lau 1992; Kripalani and Singh 1993; Kripalani and Kulkarni 1997; Zhang 1999; Krishnan and Sugi 2001; Wang et al. 2001, 2003; Ding and Wang 2005; Hu et al. 2005; Liu et al. 2008; Ogasawara and Kawamura 2008) or the North Pacific SST variability (Kawamura 1994; Park and Schubert 1997; Lau et al. 2000, 2004a, b; Lau and Weng 2002). Ding and Wang (2005) identified a circum global teleconnection (CGT) pattern during the NH summer which links regional teleconnection patterns such as the Indian summer monsoon (ISM)-East Asian summer monsoon (EASM) (Kripalani and Kulkarni 1997; Wang et al. 2001; Krishnan and Sugi 2001; Wu and Wang 2002) or the “silk road” teleconnection (Enomoto et al. 2003) pattern, and the western North Pacific-North America (Wang et al. 2001), or Tokyo-Chicago express (Lau et al. 2004a) teleconnection pattern. In spite of the fact that teleconnection patterns in boreal summer are weaker than their winter counterpart, the previous studies demonstrated that those patterns are intimately related to surface temperature and precipitation variability in the NH extratropics and may act as a significant source of climate variability and predictability over the extratropical region of interest.

How to determine the fractional signal variance (the predictable part of total variance) and predictability of atmospheric variability on seasonal time scale is still an open issue. According to the conventional signal-to-noise ratio approach (Charney and Shukla 1981; Shukla 1998; Rowell 1998; Kang and Shukla 2006) with ensemble simulations of a stand-alone atmospheric model, summertime atmospheric variability in the NH extratropics is less predictable than its winter counterpart and far less than that in the tropics. However, predictability obtained from the AGCM-alone approach is highly model-dependent. To better estimate predictability of seasonal-to-interannual climate variations, Wang et al. (2007) suggested a

“predictable mode analysis” approach, which relies on identification of the predictable leading modes of the interannual variations in observations and retrospective MME forecast. The predictability is estimated by the fractional variance accounted for by the predictable leading modes. The present study attempts to apply this approach to investigate the predictability of the upper tropospheric circulation in the NH extratropics during June–July–August (JJA).

Ding and Wang (2005) identified two dominant empirical orthogonal function (EOF) modes of interannual variability of JJA geopotential height (GPH) at 200 hPa in the NH and proposed that the second EOF mode (The so-called CGT mode) could be a major source of climate variability and predictability in the NH extratropics. Here we further investigate the predictability of these modes by comparison of observation and the MME prediction. The MME prediction was made based on three coupled models’ retrospective forecast data from National Centers for Environmental Prediction (NCEP), Geophysical Fluid Dynamic Lab (GFDL) in the USA, and Centre for Australia Weather and Climate Research (CAWCR) in Australia which have participated in the APEC Climate Center/Climate Prediction and its Application to Society (CliPAS) project (Wang et al. 2009; Lee et al. 2010). All coupled models have retrospective forecast targeting JJA mean prediction as a function of forecast lead month from five (January 1st initial condition) to zero (June 1st initial condition) for the 25-year period of 1981–2005.

Section 2 introduces the observation and prediction data used in this study. In Sect. 3, the current status of dynamical prediction for JJA climate anomalies is investigated including 200-hPa GPH, 2 m air temperature, and precipitation. Section 4 is devoted to identification of the predictable modes of JJA 200-hPa GPH in the NH and investigation of predictability and realizable forecast skill for the predictable modes. Climate anomalies associated with the predictable modes are examined in Sect. 5. Section 6 summarizes this study.

## 2 Data and analysis method

### 2.1 Retrospective forecast data

The fully coupled ocean-land-atmosphere models used in this study are NCEP Climate Forecast System (CFS), GFDL Couple Model Version 2.1 (CM2.1) and CAWCR Predictive Ocean-Atmosphere Model for Australia (POAMA) Version 1.5. Each modeling center generated retrospective forecast for the common period of 1981–2005, which were initiated every month with an integration of more than 9 months. All models do not apply any flux

correction. NCEP CFS and CAWCR POAMA have their own ocean data assimilation (ODA) scheme for ocean initialization, but they use the different methods for atmospheric initialization. GFDL CM2 has a fully coupled data assimilation (CDA) system (Zhang et al. 2007, 2008). A brief summary of the coupled models and their retrospective forecast is presented in Table 1.

The atmospheric and oceanic components of the CFS are the NCEP atmospheric Global Forecast System (GFS) model (Moorthi et al. 2001) and the GFDL Modular Ocean Model version 3 (MOM3; Pacanowski and Griffies 1998), respectively. The hindcast has 15 atmospheric initial conditions that have different starting dates. The first (second) set of 5 atmospheric initial states from 9th to 13th (from 19th to 23rd) used the same pentad ocean initial condition as the 11th (21st). The last set of 5 atmospheric initial states include the second-to-last day of the month, and the first, second, and third days of the next month. Since the first 5 members started 20 days earlier than forecast target month, we tested the sensitivity of results on the choice of ensemble members by obtaining ensemble mean using all 15 members, 10 members excluding the first set of 5, and the last set of 5 members. It is found that an increase in the number of ensemble members from 5 to 15 has little effect on improving or degrading seasonal climate forecast skill. Thus, all 15 members are used for constructing ensemble mean forecast anomalies. For convenience, we will refer the forecast starting date of the latest three members to initial condition. For example, CFS ensemble mean forecast with May initial condition actually includes forecast members initiated from 9–13th, 19th–23rd and 29–30th of April and 1–3rd of May.

The GFDL CM2 system consists of AM2p12 (AM2/LM2; GFDL Global Atmospheric Model Development Team 2004) and the fourth version of the Modular Ocean Model (MOM4; Delworth et al. 2006). Using Coupled Ensemble Data Assimilation (CDA) system (Zhang et al. 2007, 2008), GFDL CM2 produced 10 ensemble simulations initiated from the first day of every month with an integration of 12 months. All 10 ensemble members are used to calculate ensemble mean prediction.

The POAMA version 1.5 system used in this study includes the Australian Community Ocean Model version 2 (ACOM2) and the Bureau of Meteorology Research Centre Atmospheric Model version 3 (BAM3) (Alves et al. 2003). Its retrospective forecast has 10 ensemble simulations initiated from the first day of every month with different initial condition from an Atmosphere-Land Initialization (ALI; Hudson et al. 2010) scheme and same ocean initial conditions from ODA system. The ensemble mean from 10 members is used to assess seasonal prediction skill of POAMA.

The MME prediction was made by simply averaging of the three coupled models' ensemble means for targeting JJA seasonal prediction with six consecutive initial months from January (5-month forecast lead) to June (0-month forecast lead).

## 2.2 Observed data

The observed data used are obtained from the climate prediction center (CPC) merged analysis of precipitation (CMAP) data set (Xie and Arkin 1997) for precipitation, from the NCEP/department of Energy (DOE) reanalysis II data (Kanamitsu et al. 2002) for 2 m air temperature, 200-hPa zonal wind, and 200-hPa GPH, and from the improved Extended Reconstructed Sea Surface Temperature Version 2 (ERSST V2) data (Smith and Reynolds 2004) for SST.

## 2.3 Forecast quality measures

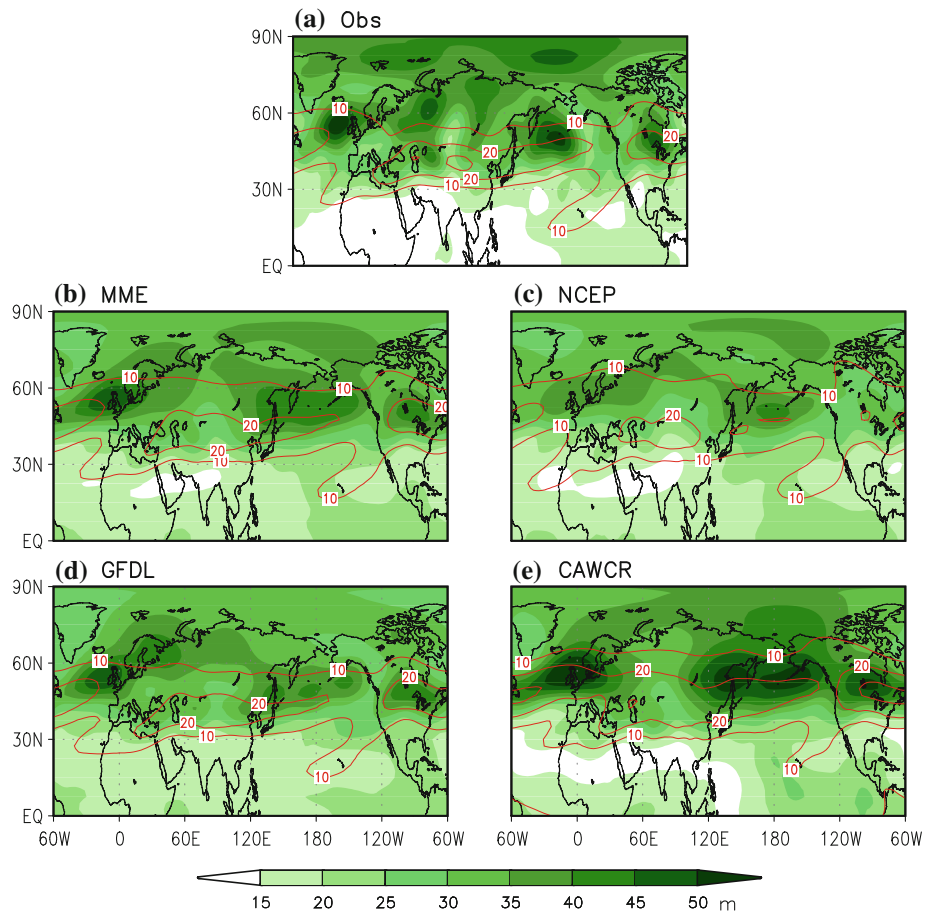
The measure of prediction skill includes the temporal correlation coefficient (TCC) skill for temporal variation and anomaly pattern correlation coefficient (PCC) skill for spatial similarity. We also calculated the area-averaged TCC skill over the NH tropics (Eq–30°N) and extratropics (30°–80°N), respectively, taking latitudinal weight into account.

We define a skill score as representing the coupled models' capability in predicting EOF modes in terms of the PCC score for eigenvector and TCC score for the principal component (PC) time series for each mode. The skill score for each mode ( $i$ ) is calculated by

**Table 1** Description of the coupled models and their retrospective forecast used in this study

Institute (model name)	AGCM	OGCM	Ensemble member	Period and forecast lead time	Reference
CAWCR (POAMA1.5)	BAM 3.0d T47 L17	ACOM2 0.5–1.5°lat × 2° lon L31	10	1980–2006, 9 months	Zhong et al. (2005)
GFDL (CM2.1)	AM2.1 2°lat × 2.5°lon L24	OM3.1 (MOM4) 1/3° lat × 1° lon L50	10	1979–2005, 12 months	Delworth et al. (2006)
NCEP (CFS)	GFS T62 L64	MOM3 1/3° lat × 1° lon L40	15	1981–2008, 9 months	Saha et al. (2006)

**Fig. 1** Standard deviation of the JJA geopotential height (*shading*) and zonal wind (*contour*) at 200 hPa obtained from **a** observation and the 1-month lead seasonal prediction of **b** MME, **c** NCEP, **d** GFDL, and **e** CAWCR. The unit is m for geopotential height and  $\text{m s}^{-1}$  for zonal wind



$$\text{Skill Score } (i) = \sqrt{\text{PCC}(i) \times \text{TCC}(i)}.$$

The skill score ranges from 0 (no skill at all) to 1 (for perfect forecast). It should be mentioned that we reordered the EOF modes of the MME prediction according to the skill score because the order of the predicted EOF mode is not necessarily the same as its observed counterpart. In order to reorder the predicted EOF modes, the skill score for the first observed mode was first calculated against all of the predicted modes and then the predicted mode that had the best skill score with the first observed mode was taken as the first predicted mode. Repeating the above process, other predicted modes were similarly determined. In the case of 200-hPa JJA GPH, there was no change of mode order until the 4th predicted mode. The predicted modes higher than the 4th mode have a different order from their observed counterpart.

### 3 Evaluation of the prediction of JJA extratropical climate

In this section we assess the current status of seasonal prediction of JJA extratropical climate including upper-

tropospheric circulation especially with May initial conditions (1-month lead).

Figure 1 compares the observed and simulated interannual variability of upper-level circulation along with the climatological jet stream in JJA. Individual ensemble simulations of each model are used to estimate standard deviation of the JJA 200-hPa GPH for individual models and their MME. In observation, major variability centers are found over the northeast Atlantic Ocean and Western Europe, central Asia, the North Pacific, and northern North America (Fig. 1a). The variance is prominent in the jet exit regions over the North Atlantic and North Pacific. The three coupled models and their MME capture, to some extent, the location of summertime jet streams, but have difficulty in capturing the observed variability centers except over the Northeast Atlantic and Western Europe and northern North America. In particular, the variability center over the North Pacific in MME prediction is shifted westward compared to the observed counterpart.

Figure 2 shows the JJA seasonal forecast skills over the NH extratropics with May initial condition for the three coupled models and their MME prediction for the period of 1981–2005. The skills for 200-hPa GPH are much lower over the extratropics than those over the tropics (Fig. 2a)

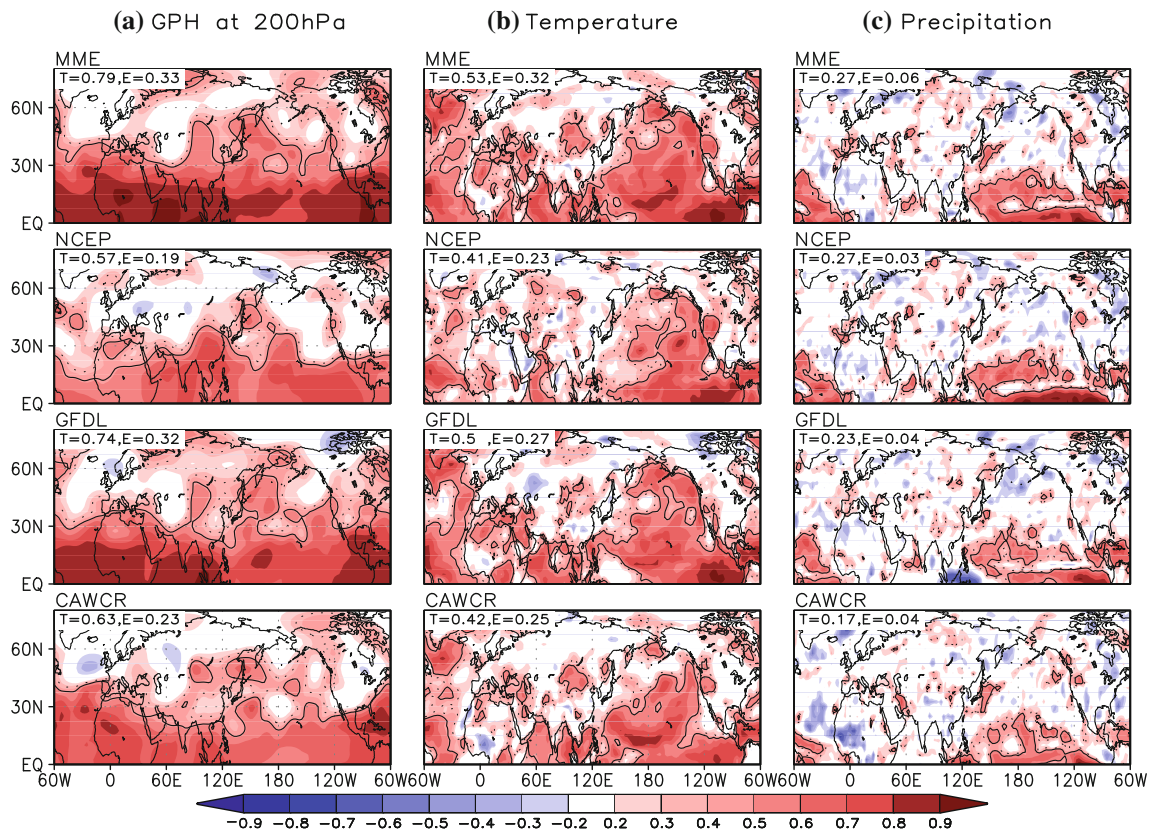


**Fig. 2** The temporal correlation coefficient (TCC) skill for the 1-month lead JJA prediction of **a** 200-hPa geopotential height (GPH), **b** 2 m air temperature, and **c** precipitation with May 1st initial condition obtained from three coupled models and their multi-model ensemble (MME) for the period of 1981–2005 in the Northern

Hemisphere. *Solid (dashed) line* represents statistical significance of the correlation coefficients at 95% (99%) confidence level. The *numbers in the left upper corners* indicate averaged correlation skill over the tropics (T, 0–360°E, Eq–30°N) and extratropics (E, 0–360°E, 30–80°N) in the NH

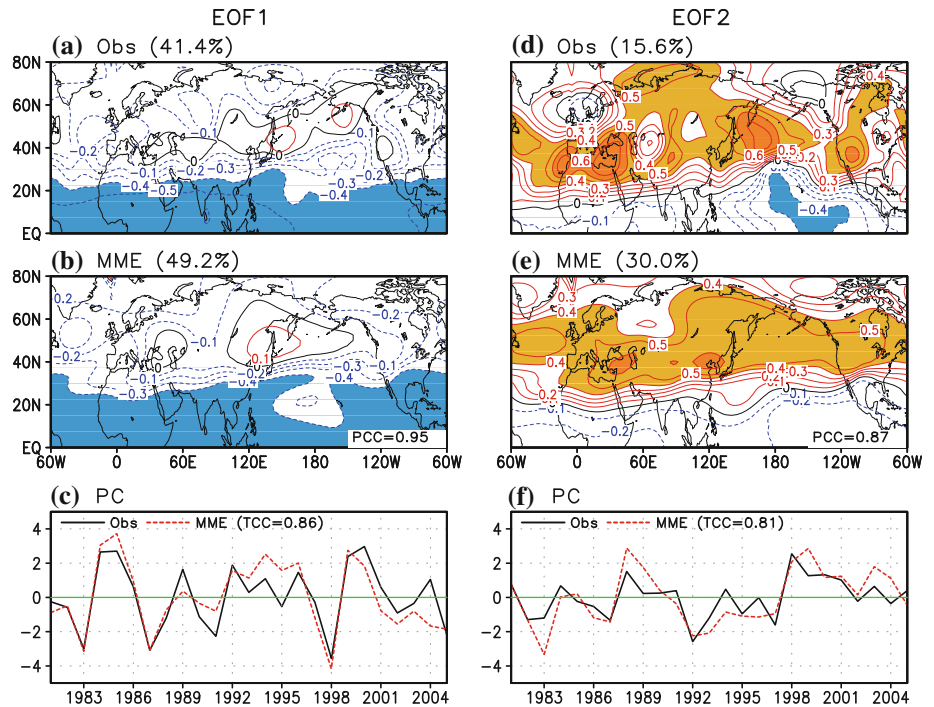
and are consistent with earlier results (Peng et al. 2000) The area-averaged TCC skill for 200-hPa GPH of the MME prediction is 0.79 over the NH tropics and 0.33 over the extratropics. Individual coupled models have lower skill than the MME. GFDL CM2.1 has the best skill of 0.74 over the tropics and of 0.32 for the extratropics. Nonetheless, the MME and individual coupled models have significant skills over some geographical locations including East Asia, its adjacent ocean, and the west coast of the North America and North Atlantic, suggesting that predictable patterns (or modes) of the JJA upper-level circulation in the NH extratropics may exist. Significant forecast skill is also observed for 2 m air temperature (Fig. 2b) and precipitation (Fig. 2c) over some specific locations of the NH extratropics. It is interesting to note that there are specific locations in which all coupled models tend to have significant forecast skills. For instance, the coupled models have some forecast skill in precipitation over some parts of the East Asian monsoon region, Central Europe, and western North America, although they have almost zero TCC skill on average over the NH extratropics. It is of importance to understand the source of the prediction skill

in the current coupled models and to identify predictable modes of climate variability.

Next, we evaluate how well the MME hindcast captures the first two dominant modes of variability of the 200-hPa GPH in JJA. To identify the major modes of summertime upper-tropospheric atmospheric circulation, we first applied EOF analysis, using the correlation matrix, to the JJA 200-hPa GPH over the entire NH (0–360°E, Eq–80°) in observation and in the MME prediction with May initial condition. All data were interpolated to the same geographic grid to avoid from the latitudinal weighting effect.

The first observed EOF mode (EOF1), which accounts for 41.4% of total variance, is characterized by an overall zonally oriented mode of variability of negative height anomalies (Fig. 3a). However, along the latitude circle of 50°N, positive height anomalies extend from East Asia across the entire North Pacific to the western US. The associated PC time series (PC1) shows strong interannual variability with a time scale of 3–6 years and indicates that the EOF1 has significant variability associated with the decay of ENSO in JJA, after the mature phase of ENSO, such as JJA 1983, 1987, and 1998 (Fig. 3c).

**Fig. 3** Spatial patterns of the first (left panels) and second (right panels) eigenvectors of 200-hPa GPH anomalies obtained from observation (a, d) and 4-coupled modes' MME prediction (b, e), respectively. c, f The principal components (PCs) of the first and the second EOF modes obtained from observation (black solid line) and MME (red dashed line). The numbers in the right lower corners in (d) and (e) indicate pattern correlation coefficient (PCC) between observation and the corresponding prediction. The numbers within the parenthesis in the figure legend in the lower panels indicate the temporal correlation coefficients (TCC) between the observed and MME PC time series



The second observed EOF mode (EOF2), which accounts for 15.6% of total variance, features both zonally symmetric distribution and a wave-like pattern (Fig. 3d). The zonally symmetric pattern is characterized by positive height over the subtropics and midlatitude and by negative height over the tropics (equatorward of 20°N). The wave-like pattern is characterized by strong positive variability over southern Europe and the Mediterranean Sea, the North Pacific, and the western part of North America. The wave-like pattern in this study is, to some extent, different from the CGT pattern by Ding and Wang (2005) which was obtained from interannual component of the 200-hPa JJA GPH variability for 56 years from 1948 to 1998. This difference indicates that there may be an interdecadal change of the CGT pattern (Wang and Wang 2010). After 1981, the variability over East Asia and the eastern part of North America weakened but that over the North Pacific and the western part of North America was enhanced. In addition, the sign of variability over northern Europe changed to negative from positive. The associated PC time series (PC2) shown in Fig. 3f indicates that the mode may have interdecadal as well as interannual variability.

The MME is capable of predicting the spatial and temporal structures of the two leading modes (Fig. 3b, c, e, f) 1-month ahead with a high fidelity. The PCC skill for spatial similarity is 0.95 for the first and 0.87 for the second eigenvector, respectively. In particular, the MME well predicts the zonal mean component of the first and second observed eigenvectors. However, it has difficulty in capturing the tilted structure over the North Pacific in the

**Table 2** Area-averaged fractional variance for the first two EOF modes over the tropics and extratropics in NH obtained from observation and the 1-month lead MME prediction

	EOF1		EOF2	
	Tropics (%)	Extratropics (%)	Tropics (%)	Extratropics (%)
Obs	76.8	13.4	7.2	22.0
MME	81.1	25.4	9.0	45.1

observed EOF1 and the aforementioned CGT pattern in the observed EOF2. The MME also well predicts the time variation of the PC1 (PC2) with a TCC skill of 0.86 (0.81). The strong positive and negative years for the PC1, such as 1983, 1987, 1998, and 1999 are especially well predicted. The MME captures not only interannual component but also interdecadal component of the observed PC2.

To better understand each mode's contribution to total variability over the tropics and the extratropics, the area-averaged fractional variances over the two regions were calculated and the results are presented in Table 2. Fraction variance of each mode is defined by the ratio of eigenvector multiplied by square of principal component to the total variance at each grid point (Wang and An 2005). Table 2 indicates that in observation the EOF1 accounts for 76.8% (7.2%) of total variance over the tropics (extratropics) in observation and thus represents the tropical atmospheric variability, while the EOF2 has more contribution from variability over the extratropics accounting for 22.0% of total variance. This result is consistent with the results of

Ding and Wang (2005) who emphasized the observed second EOF mode as the CGT mode in the extratropics. The 1-month lead MME prediction captures similar fractional variance of its total variability with the observed counterpart over the tropics, which is 81.1% for the EOF1 and 9.0% for the EOF2, respectively. On the other hand, the MME overestimates the fractional variance over the extratropics which is 25.4% (45.1%) for the EOF1 (EOF2) and is twice the observed counterpart for both modes, indicating significant reduction of higher modes' variance during the ensemble averaging process.

#### 4 Predictability of the JJA 200-hPa GPH

##### 4.1 Identification of predictable modes

In this study, a way to determine predictable modes is suggested using observation and the state-of-the-art climate model's predictions based on Wang et al. (2007). There are two basic criteria for the determination. First, in observation, predictable modes should explain a large part of the total variability and be statistically separated from other higher modes. Second, the climate prediction models should be capable of predicting these major modes. According to the criteria, the predictable modes are identified using percentage variance for each EOF mode in observation and the skill score of the MME prediction in terms of the PCC skill for eigenvector and the TCC skill for the PC time series for each mode as defined in Sect. 2.3.

Figure 4 shows a scatter diagram between the observed percentage variance (ordinate) and the skill score for each EOF (abscissa) mode. The first two modes are not only well separated from higher modes statistically but also predicted with high fidelity by the current coupled models' MME. The current MME cannot predict higher modes. Thus, we consider the first two leading modes as predictable modes for interannual variability of 200-hPa JJA GPH. The first two modes capture about 57% of the observed total variability and 79.2% of the predicted total variability over the NH with a forecast skill score of 0.92 for the EOF1 and 0.84 for the EOF2, respectively. Over the extratropics only, 35% (70.5%) of the observed (predicted) total variability can be explained by the first two modes.

##### 4.2 Prediction skill and realizable potential predictability

This subsection describes the current level of prediction skill that is attained by the 1-month lead MME prediction along with a discussion of potential predictability, which can be achieved using the first two predictable modes. Given the assumption that the first two leading modes are

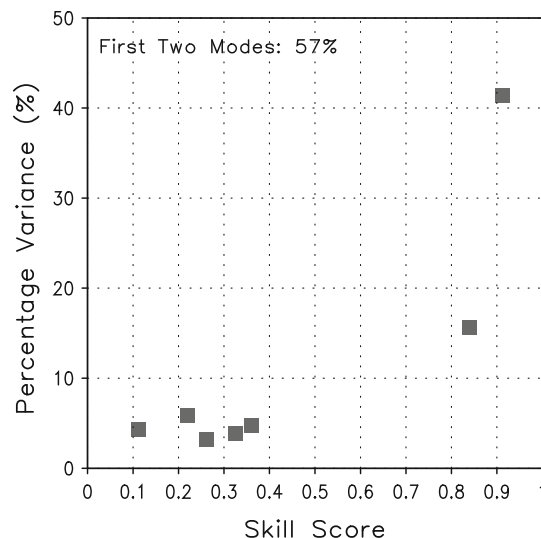


**Fig. 4** The percentage variances that are accounted for by the observed first seven EOFs (ordinate) and the combined forecast skill score for the eigenvector and principal component for each mode (abscissa) for 200-hPa GPH in NH. The leading two modes of the observed 200-hPa GPH in JJA capture about 57% of the total interannual variability

more predictable and the higher modes are less predictable (Fig. 4), the total predicted as well as observed fields are decomposed into the predictable and unpredictable parts. The predictable part is reconstructed by the linear combination of the first two EOF modes and the unpredictable part is then calculated by subtracting the predictable part from the total field.

Figure 5a shows the TCC skill of the 1-month-lead MME prediction which comes primarily from the prediction skill with the first two predictable modes shown in Fig. 5b. In general, the contribution from the residual higher modes for the MME prediction is insignificant because they only contribute slightly positively over the subtropics but slightly negatively over the midlatitude (Fig. 5c). The results imply that most of the MME skill comes from the coupled model's capability in predicting the first two modes.

From a conventional point of view, potential predictability can be defined by the fractional variance of the predictable part. In this case, about 84% (35.4%) of total variability is potentially predictable over the NH tropics (extratropics). In this study, however, the realizable potential predictability is estimated by the TCC between the observed total field and the observed predictable part in order to facilitate comparison with the MME prediction skill. Thus, it represents the achievable forecast skill if climate prediction models can perfectly predict the observed predictable modes.

Figure 5d shows, as defined above, the potential predictability of the 200-hPa JJA GPH, which indicates that

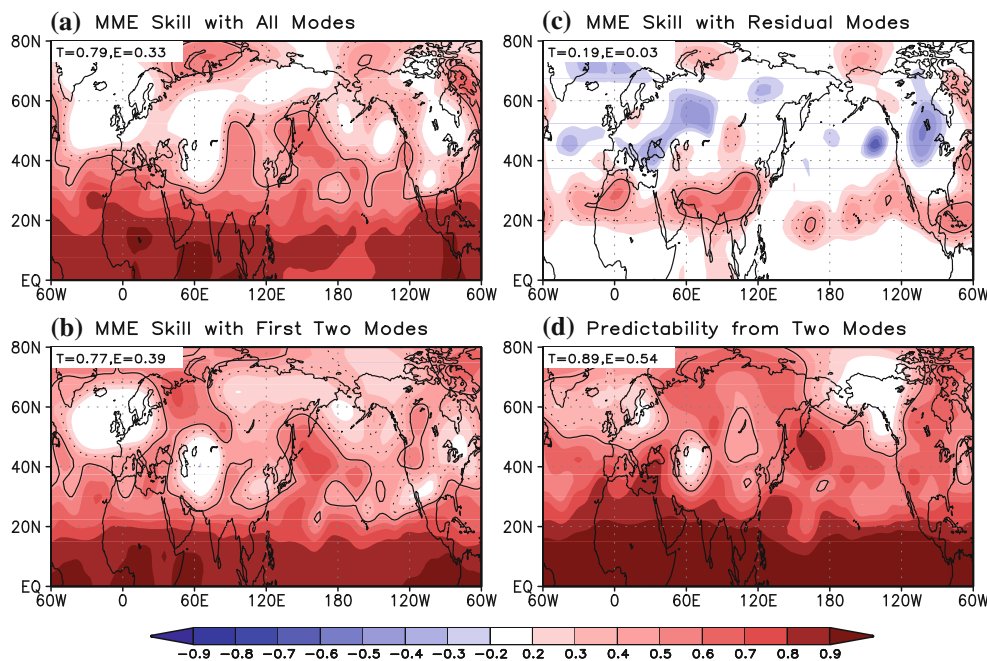


**Fig. 5** MME prediction skill for 200-hPa JJA GPH using **a** total field, **b** reconstructed field from the first two modes, and **c** reconstructed field from higher mode. **d** Potential predictability estimated for the 200-hPa JJA GPH from the observed first two EOF modes. *Solid (dashed) line* represents statistical significance of the correlation

coefficients at 95% (99%) confidence level. The *numbers* in the *left upper corners* indicate averaged correlation skill over the tropics (T, 0–360°E, Eq–30°N) and extratropics (E, 0–360°E, 30–80°N) in the NH

the interannual variability over particular geographic locations in the NH extratropics is significantly predictable associated with the first two EOF modes in spite of the fact that the extratropical upper-tropospheric circulation is generally much less predictable than that over the tropics. The locations with significant predictability over the NH extratropics include the Northwest Pacific, most of North America, southern Europe and the Mediterranean Sea in which the prominent variability of the observed second eigenvector (Fig. 4d) is observed. Wherever the variability of the second eigenvector is weak, the potential predictability is also low such as over northern Europe, Central and East Asia, and Alaska.

Obviously, the 1-month-lead MME prediction skill shown in Fig. 5a is far below the potential predictability over the extratropics. Nonetheless, the predictable part of the MME prediction (Fig. 5b) better predicts the observed variability where the potential predictability is higher.

#### 4.3 Long-lead prediction of the predictable modes

We further investigate the prediction skill with different lead for the 200-hPa JJA GPH anomalies and its predictable modes in comparison with the aforementioned 1-month lead prediction skill. Figure 6 shows the TCC skill of the MME prediction for interannual variability of the 200-hPa GPH in JJA as a function of forecast initial month

(forecast lead time) from January (5 month) to June (0 month), respectively. It is interesting to note that the TCC skill over the tropics gradually increases as forecast lead time decreases while over the extratropics the skill doesn't significantly depend on the forecast lead time. Even when initiated from January, the MME skills over Southern Europe, some parts of East Asia, and the western part of the North Pacific are as good as the 1-month lead. This seems to imply that the JJA extratropical prediction skill may depend on overall prediction skill of ENSO events (which have useful skill up to 6 months in the MME), but not the detailed evolution of the ENSO events.

As is the case for the 1-month lead prediction, the long-lead skill of MME prediction comes from successful prediction of the two predictable modes. Figure 7 shows that the MME captures the spatial pattern of EOF1 well, regardless of forecast lead time, with the PCC score ranging from 0.94 to 0.97. However, the TCC score for the PC1 decreases with lead time from 0.81 (0-month lead) to 0.62 (5-month lead). Note that the long-lead MME forecast is superior for strong variability years, such as 1984, 1998, and 1999, but it is particularly poor during weak years such as 1993–1995 and 2002–2005.

As for EOF 2, the MME captures the zonally symmetric pattern of the observed second mode well even 5 months ahead, but it has difficulty in capturing the zonally asymmetric CGT pattern regardless of forecast

**Fig. 6** Spatial pattern of the TCC skill of MME prediction for 200-hPa GPH in JJA as a function of forecast initial month from January (a) to June (f). Solid (dashed) line represents statistical significance of the correlation coefficients at 95% (99%) confidence level

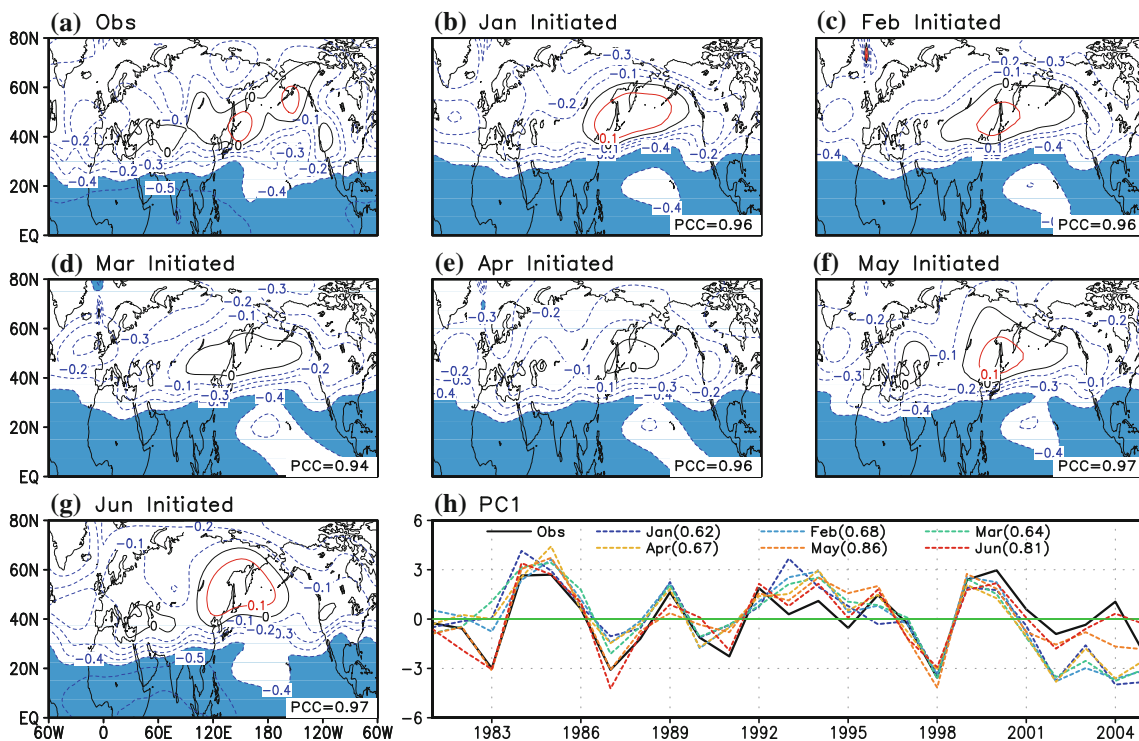
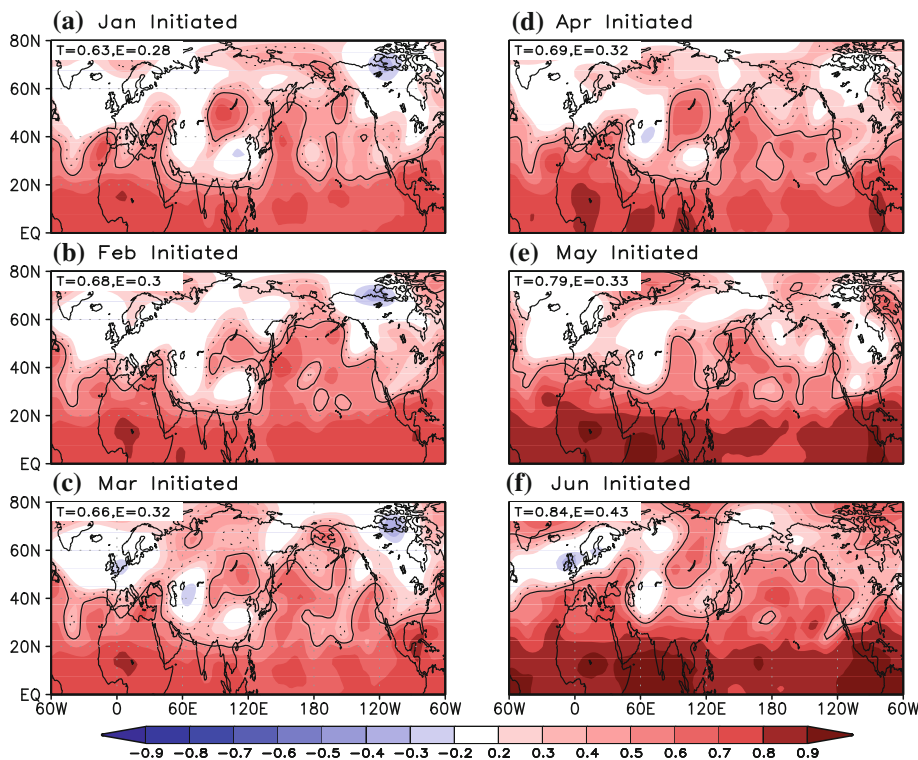


**Fig. 7** Spatial patterns (a–g) and principal component (h) of the first EOF mode of 200-hPa GPH anomalies obtained from observation and MME prediction with initial month from January to June, respectively. The numbers in the right lower corners in (b) through

(g) indicate PCC between the observed and the corresponding eigenvectors. The numbers within the parenthesis in the figure legend of (h) indicates TCC between the observed and predicted PC time series

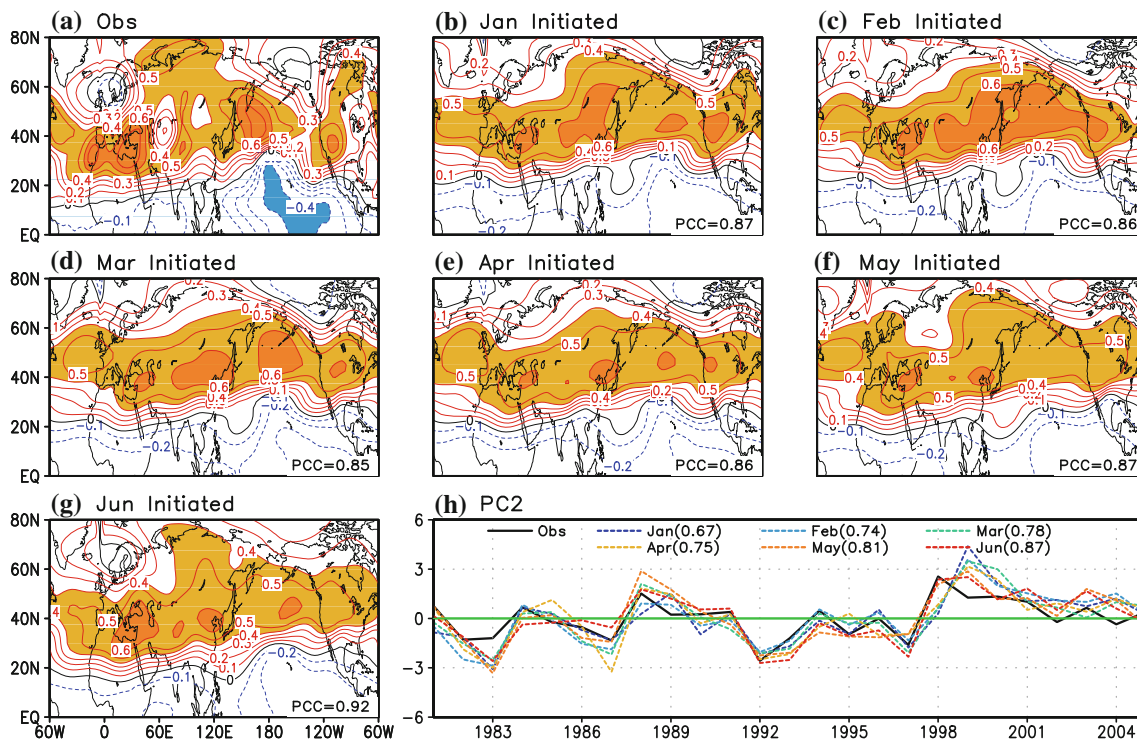


**Fig. 8** Spatial patterns (a–g) and principal component (h) of the second EOF mode of 200-hPa GPH anomalies obtained from observation and MME prediction with initial month from January to June, respectively. The numbers in the right lower corners in

(b) through (g) indicate PCC between the observed and the corresponding eigenvectors. The numbers within the parenthesis in the figure legend of (h) indicates TCC between the observed and predicted PC time series

lead time (Fig. 8). On the other hand, the interdecadal trend as well as interannual variability of the PC2 are reasonably well predicted even 5 months ahead with a TCC skill of 0.67.

The results in this subsection point out that the current generation of coupled models can predict summertime variability well over specific locations in the NH extratropics even 5 months ahead and the long-lead predictability relies on the coupled model's capability in capturing the first two predictable modes.

#### 4.4 Source of predictability

Given the fact that the current coupled models predict the first two EOF modes with a high fidelity even 5 months ahead, one may wonder what the sources of predictability are. Figure 9a shows the lead-lag correlation coefficients for seasonal mean SST against the first PC, which reveals that the climate predictability of the first mode comes mainly from ENSO in observation. Strong negative correlation over the Central and Eastern Tropical Pacific appears during the previous DJF (2 seasons before), indicating that a strong positive (negative) phase of the EOF1 tends to occur during the summers after the mature phase of La Niña (El Niño). The relationship seems to explain

long-lead predictability of the EOF1, along with the fact that the climate prediction models tend to predict well climate anomalies in JJA after the mature phase of ENSO as shown in Wang et al. (2009). Previous studies indicated that the prolonged impact of ENSO on the western North Pacific and East Asian monsoon is due to either local warm pool ocean-monsoon interaction (Wang et al. 2000) or the capacity effect of the Tropical Indian Ocean (Xie et al. 2009; Chowdary et al. 2010a, b). The local warm pool ocean-monsoon interaction maintains the Philippine Sea anticyclonic anomaly formed during the mature phase of El Niño (Wang et al. 2000). The anomalous monsoon precipitation is therefore important for the tropical-extratropical interaction over the North Pacific sector. The delayed warming over the Indian Ocean may also contribute to the zonally symmetric anomalies of the EOF 1 (Kumar and Hoerling 2003; Seager et al. 2003). Xie et al. (2009) further demonstrated that the persistent Indian Ocean warming after the mature phase of ENSO plays an important role on the western North Pacific climate through the Kelvin wave-induced Ekman divergence mechanism and the intensification of the subtropical westerly jet.

Further analysis indicates that the second mode has two different predictability sources (Fig. 9b). On the interannual time scale, ENSO probably regulates the second

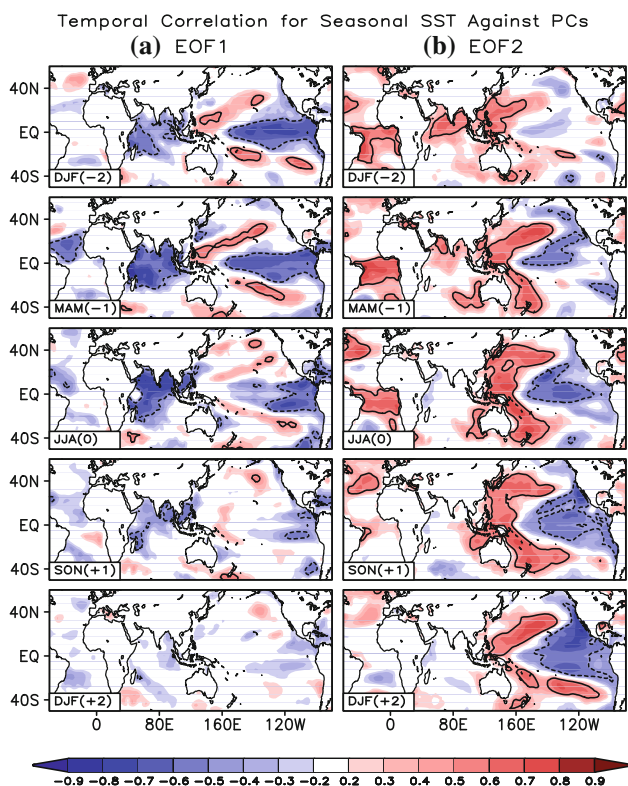


**Fig. 9** Spatial patterns of the lead-lag correlation coefficients for seasonal mean SST against (a) the first PC and (b) the second PC, respectively, obtained from observation. Correlation coefficients which are statistically significant at 99% confidence level are contoured

mode. For example, the strong positive (negative) phase of the EOF2 occurs during the summer of developing the La Niña (El Niño) event. Thus, the forecast quality for the JJA SST over the central and eastern Pacific concurrent with the PC2 may play an important role in better predicting the interannual component of EOF2. The TCC skill for the JJA Nino 3.4 SST index reaches 0.71 at 5-month lead and gradually increases to 0.91 as the forecast lead time decreases to 0-month lead and may contribute to the lead-time dependency in skill for predicting this mode.

On the interdecadal time scale, the SST anomalies over the Western Tropical Pacific (WTP), North Pacific (NP), and North Atlantic (NA) have significant positive correlation with PC2 shown in Fig. 9b. The SST anomalies in the aforementioned regions exhibit stronger interdecadal variability than interannual variability (not shown) and have significant correlation with each other (Table 3). It is further found that the coupled models' MME has long-lead predictability for those SST anomalies. Unlike from the forecast skill for the JJA Nino 3.4 SST anomalies characterized by a gradual decrease with increasing forecast lead time, the skill for the SST anomalies over the aforementioned three Oceanic regions exhibits the best skill at 3- or

**Table 3** Temporal correlation coefficients between area-averaged JJA SST indices

	Nino3.4	TAO	WTP	NP	NA
Nino3.4	1	<b>-0.55</b>	-0.37	-0.32	-0.4
TAO		1	<b>0.6</b>	0.36	<b>0.63</b>
WTP			1	<b>0.79</b>	<b>0.73</b>
NP				1	<b>0.73</b>
NA					1

The Nino 3.4 index is obtained from area-averaged SST over 5°S–5°N, 150°–90°W, the Tropical Atlantic Ocean (TAO) index over 10°S–Eq, 60°–10°W, the Western Tropical Pacific (WTP) index over 5°–20°N, 130°–160°E, the North Pacific (NP) index over 25°–45°N, 120°E–160°W, and the North Atlantic (NA) index over 30°–45°N, 60°–20°W. The bold value indicates that the correlation coefficient is statistically significant at 99% confidence level

4-month lead. In the case of the NP SST anomaly, the MME has the best TCC skill of 0.88 at 3-month lead and the lowest skill of 0.65 at 1-month lead which probably provides an important source for long-lead predictability of EOF2. Further study is needed to better understand the interdecadal change of the second EOF mode and the role of SST over the three oceanic regions.

### 5 Associated surface climate anomalies

Ding and Wang (2005) showed that the CGT mode is also accompanied by significant rainfall and surface air temperature anomalies over the NH extratropics. We further analyze the climate anomalies associated with the first two predictable modes in observation and the 1-month lead seasonal prediction.

Figure 10 shows the spatial distribution of the correlation coefficients for JJA 2 m air temperature and precipitation, respectively, against the first PC time series along with the first eigenvector, which was obtained from observation and the MME prediction with May initial condition. In observation, the 2 m air temperature anomaly concurrent with the first mode is characterized by significant cooling over the most part of the NH including South Asia and the eastern part of North America and regional warming over northern East Asia and the adjacent Ocean and the western US. The MME captures anomalies over the Subtropics well but fails to predict anomalies over the extratropics including North America and some parts of Eastern Europe (Fig. 10b). The warm anomaly over East Asia and the adjacent ocean is also slightly shifted northward.

The most striking precipitation anomaly associated with the first mode is seen over East Asia and its adjacent North Pacific Ocean in observation, which is a zonally oriented pattern of positive and negative anomalies

**Fig. 10** Spatial distribution of the first eigenvector (*contour*) and the correlation coefficients (*shading*) between JJA 2 m air temperature (*left panels*) and precipitation (*right panels*) and the first PC obtained from observation (*upper panels*) and MME (*lower panels*)

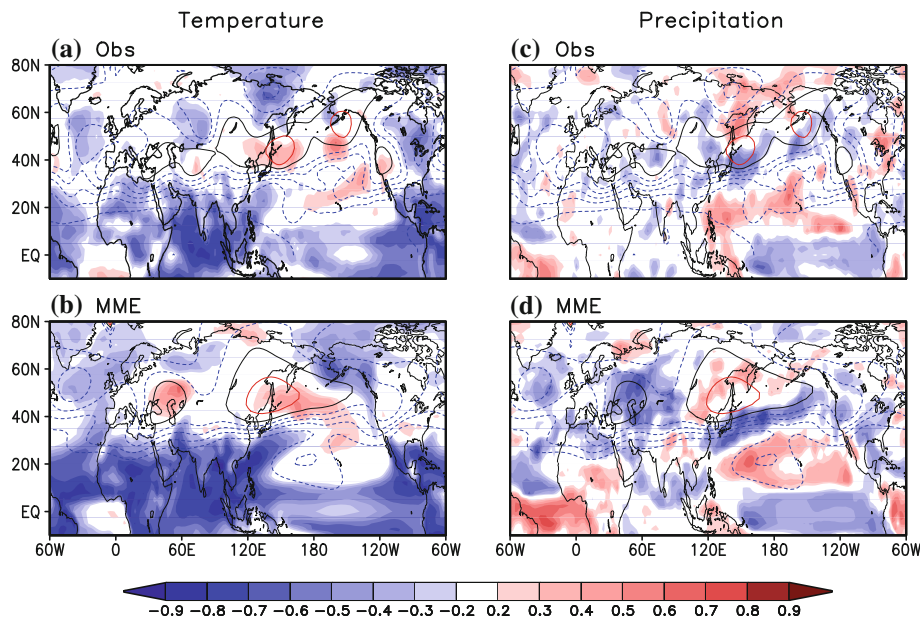


**Fig. 11** Spatial distribution of the second eigenvector (*contour*) and the correlation coefficients (*shading*) between JJA 2m air temperature (*left panels*) and precipitation (*right panel*) and the first PC obtained from observation (*upper panels*) and MME (*lower panels*)

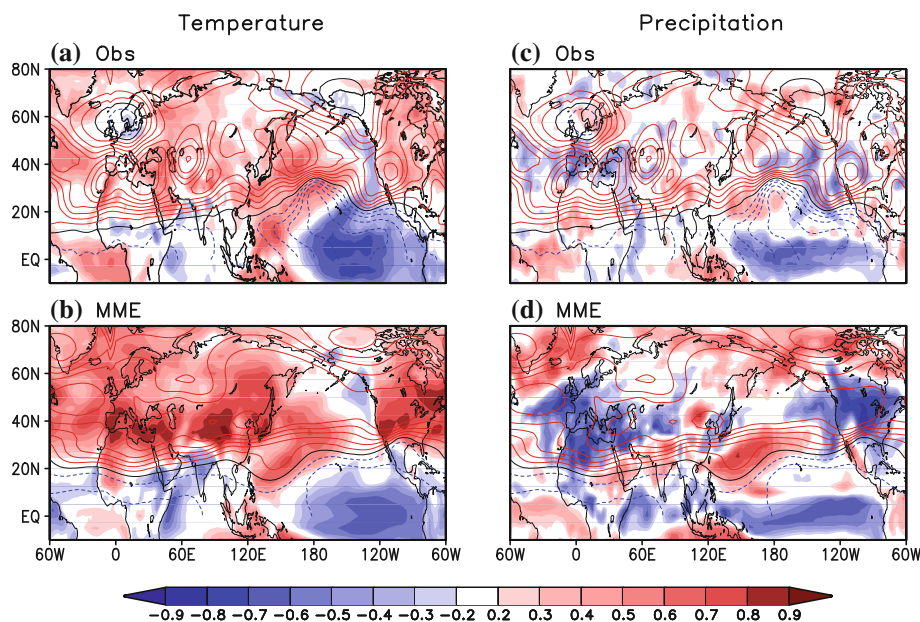


(Fig. 10c). The MME captures the anomaly pattern over East Asia and the adjacent Ocean well but is not successful in predicting the anomaly over the Philippine Sea and the South China Sea, Indochina, Eastern Europe, and eastern North America. It is suggested that the seasonal climate prediction for precipitation over East Asia may benefit most from the link to EOF1 in the current MME prediction.

Associated with the positive phase of the EOF2, most of continental regions over the extratropics show positive anomaly in the 2 m air temperature except northern Europe, north-eastern Russia and Alaska (Fig. 11a). The MME exaggerates warm anomalies over most of the conti-

mental midlatitude and fails to capture cooling anomalies over northern Europe (Fig. 11b). In addition, The MME shows significant cooling anomaly over India that is not shown in the observation.

While the TCC for the observed 2 m air temperature (Fig. 11a) against EOF2 has zonally symmetric distribution and significant value over the most continental regions, the TCC for the observed precipitation shows a localized distribution with moderate amplitude (Fig. 11c). Significant negative TCC is found over central and southern Europe, western North America-eastern North Pacific, and the positive TCC is shown over southern China. In general, the MME overestimates the amplitude of the TCC (Fig. 11d),

as expected, because the MME procedure reduces noise variance of the prediction. The MME well captures the strong negative anomaly over central and southern Europe and eastern North Pacific-western North America, but the negative anomalies are too strong and cover too-large areas. The positive anomalies over India are opposite to the observed anomalies. It is interesting to note that the MME has strong relationship between the Indian precipitation and the CGT mode which is not present in the observation as discussed in Sect. 3. In observation, the CGT mode tends to be concurrent with the ENSO but not the Indian rainfall. On the other hand, in the MME, it is strongly related to not only the ENSO but also to the Indian rainfall anomaly. Taken together, successful prediction of the EOF2 in the MME seems to add some forecast skill for precipitation over central and southern Europe. However, the MME's failure to capture the detailed wavelike structure of the CGT mode results in failure in predicting precipitation over most parts of the extratropical continents.

## 6 Conclusion

How to estimate seasonal climate predictability is still an open issue, especially in terms of coupled climate models. In this study, we suggest a way to estimate predictability of upper-tropospheric atmospheric variability. This method relies on identification of predictable modes using both observation and the state-of-the-art dynamical multi-model ensemble hindcast. The data used are 200-hPa GPH in JJA obtained from NCEP/DOE reanalysis II and three coupled modes' hindcast from NCEP, GFDL, and CAWCR for 25 years of 1981–2005. The three coupled models' MME predicts JJA 200-hPa GPH over the tropics with a high fidelity, but has difficulties in predicting those over the NH extratropics. Nonetheless, over specific geographic locations in the extratropics, the MME has considerable forecast skill, suggesting that predictable patterns may exist over the region of interest.

We demonstrated that the seasonal forecast skill for the NH 200-hPa geopotential height in summer basically comes from the coupled models' capability to predict the first two empirical orthogonal function (EOF) modes of interannual variability. The models cannot capture the residual higher modes and hence prediction of the higher modes contributes little to the seasonal forecast skill. Strong positive (negative) phase in the first mode tends to occur during the summers after the mature phase of La Niña (El Niño), and is thus driven by prolonged impacts of the ENSO. The second mode, on the other hand, is regulated by developing phase of the ENSO on the interannual time scale and is correlated with the SST anomalies over

the North Pacific, North Atlantic, and tropical Western Pacific on the interdecadal time scale.

The first two EOF modes of the 200-hPa JJA GPH in the NH are identified as “predictable mode” for a number of reasons. First, these observed modes are statistically well separated from the higher modes and account for the large fraction of total variability; second, these modes have clear physical interpretations and their sources are understood in terms of ENSO teleconnection dynamics; and third, the current MME is capable of predicting the spatial structure and temporal variation of these modes with a high fidelity even at a 5-month lead.

Given the assumption that the first two leading modes can be perfectly predicted and the higher modes are noise patterns, we define the realizable potential predictability by the total fractional variances of the predictable modes. The observed first two modes together account more than 85% of variance over the tropics and about 35% of variance over the mid-latitudes, which may represent an upper limit for the forecast skill potentially obtainable using the improved multi-model ensemble prediction; thus offering an estimation of attainable potential predictability. Furthermore, the predictable modes provide spatial distribution of the predictable patterns, which is valuable for assessing forecast uncertainties.

Using the current MME, the 1-month lead hindcast achieves the following level of skill: The pattern correlation coefficients (PCC) between the observed and predicted eigenvector is 0.95 for the first mode and 0.87 for the second mode, and the temporal correlation coefficient (TCC) between the observed and predicted PC is 0.86 for the first mode and 0.81 for the second mode. The PCC skill for each eigenvector is not sensitive to forecast lead time but the TCC skill increases as forecast lead time decreases. The TCC skill reaches 0.6 for the first PC and 0.67 for the second mode at the 5-month lead (January initial condition).

The realizable potential predictability can also be represented by the TCC between the observed total field and the observed predictable component. Potential predictability of 200-hPa JJA GPH reveals that the interannual variability over particular geographic locations in the NH extratropics is to a large degree predictable with the first two modes, although the extratropical upper-tropospheric circulation is generally much less predictable than that over the tropics, a result consistent with earlier studies (Peng et al. 2000). Comparison between the potential predictability and the realized prediction skill reveals that (a) predictable modes of the MME prediction (Fig. 5b) better predicts the variability where the potential predictability is high, and (b) the MME prediction skill shown in Fig. 5a is far below the potential predictability over the extratropics.

The first two modes of upper level circulation are accompanied by significant JJA surface temperature and

precipitation anomalies. The most striking precipitation anomaly associated with the first mode is observed over East Asia and the North Pacific Ocean. The MME captures the anomaly over East Asia and the adjacent Ocean well but has difficulty in predicting anomalies over the Philippine Sea and the South China Sea. It is suggested that the seasonal climate prediction for precipitation over East Asia benefits most from the first EOF mode in the current MME prediction through the delayed Pacific-East Asia teleconnection by either local warm pool ocean-monsoon interaction (Wang et al. 2000) or the capacity effect of the Tropical Indian Ocean (Xie et al. 2009; Chowdary et al. 2010a, b). Successful prediction of the second EOF modes in the MME seems to add some forecast skill for precipitation over central and southern Europe and the eastern North-Pacific and western North America. However, the MME's failure to capture the detailed wavelike structure of the CGT mode results in failure to predict precipitation over the other parts of the extratropical continents, including eastern North America.

**Acknowledgments** This study has been supported by a grant from the Korean Ministry of Environment as "Eco-technopia 21 project" and the Korean Meteorological Administration Research and Development Program under grant CATER 2009-1146. Wang and Lee acknowledge support from International Pacific Research Center, which is in part supported by JAMSTEC, NOAA and NASA. The authors would like to thank Dr. Shang-Ping Xie for his valuable comments and anonymous reviewers for their time and good comments that helped improve the manuscript. This is SEOST publication number 8011 and IPRC publication number 622.

## References

- Alves O, Wang G, Zhong A, Smith N, Tseitkin F, Warren G, Schiller A, Godfrey S, Meyers G (2003) POAMA: bureau of meteorology operational coupled model seasonal forecast system. Proceedings of national drought forum, Brisbane, April 2003, pp 49–56
- Charney JG, Shukla J (1981) Predictability of monsoons. Paper presented at the Monsoon Symposium in New Delhi, India, 1977, and published in Sir Lighthil J, Pearce RP (eds) *Monsoon Dynamics*, Cambridge University Press
- Chowdary JS, Xie SP, Luo JJ, Hafner J, Behera S, Masumoto Y, Yamagata T (2010a) Predictability of northwest Pacific climate during summer and the role of the tropical Indian ocean. *Clim Dyn*. doi:10.1007/s00382-009-0686-5 (in press)
- Chowdary J, Xie SP, Lee JY, Kosaka Y, Wang B (2010b) Predictability of summer Northwest Pacific climate in eleven coupled model hindcasts: local and remote forcing. *J Geophys Res*. doi:10.1007/s00382-010-0909-9
- Delworth TL et al (2006) GFDL's CM2 global coupled climate models—part I: formulation and simulation characteristics. *J Clim* 19:643–674
- Ding Q, Wang B (2005) Circumglobal teleconnection in the Northern Hemisphere summer. *J Clim* 18:3483–3505
- Enomoto T, Hoskins BJ, Matsuda Y (2003) The formation mechanism of the Bonin high in August. *Q J R Meteorol Soc* 129:157–178
- GFDL Global Atmospheric Model Development Team (2004) The new GFDL global atmosphere and land model AM2/LM2: evaluation with prescribed SST simulation. *J Clim* 17:4641–4673
- Hu ZZ, Wu R, Kinter JL III, Yang S (2005) Connection of summer rainfall variations in South and East Asia: role of El Niño-southern oscillation. *Int J Clim* 25:1279–1289
- Hudson D, Alves O, Hendon HH, Wang G (2010) The impact of atmospheric initialization on seasonal prediction of tropical Pacific SST. *Clim Dyn* (online)
- Kanamitsu M et al (2002) NCEP dynamical seasonal forecast system 2000. *Bull Am Meteor Soc* 83:1019–1037
- Kang IS, Shukla J (2006) Dynamic seasonal prediction and predictability of the monsoon. In: Wang B (ed) *The Asian monsoon*. Springer-Paraxis, Chichester, UK
- Kawamura R (1994) A rotated EOF analysis of global sea surface temperature variability with interannual and interdecadal scales. *J Phys Oceanogr* 24:707–715
- Kripalani RH, Kulkarni A (1997) Rainfall variability over southeast Asia—Connections with Indian monsoon and ENSO extremes: new perspective. *Int J Clim* 17:1155–1168
- Kripalani RH, Singh SV (1993) Large-scale aspects of India-China summer monsoon rainfall. *Adv Atmos Sci* 10:72–84
- Krishnan R, Sugi M (2001) Baiu rainfall variability and associated monsoon teleconnection. *J Meteor Soc Jpn* 79:851–860
- Kumar A, Hoerling MP (2003) The nature and causes for the delayed atmospheric response to El Niño. *J Clim* 16:1391–1403
- Lau KM (1992) East Asian summer monsoon rainfall variability and climate teleconnection. *J Meteor Soc Jpn* 70:211–240
- Lau KM, Weng H (2002) Recurrent teleconnection patterns linking summertime precipitation variability over East Asia and North America. *J Meteor Soc Jpn* 80:1129–1147
- Lau KM, Kim KM, Yang S (2000) Dynamical and boundary forcing characteristics of regional components of the Asian summer monsoon. *J Clim* 13:2461–2482
- Lau KM, Kim KM, Lee JY (2004a) Interannual variability, global teleconnection and potential predictability associated with the Asian summer monsoon. In: Chang CP (ed) *East Asian monsoon*. World Scientific Publisher, Singapore, p 564
- Lau KM, Lee JY, Kim KM, Kang IS (2004b) The North Pacific as a regulator of summertime climate over Eurasia and North America. *J Clim* 17:819–833
- Lee JY, Wang B, Kang IS, Shukla J et al (2010) How are seasonal prediction skills related to models' performance on mean state and annual cycle? *Clim Dyn* 35:267–283
- Liu J, Wang B, Yang J (2008) Forced and internal modes of variability of the East Asian summer monsoon. *Clim Past* 4:225–233
- Moorthi S, Pan HL, Caplan P (2001) Changes to the 2001 NCEP operational MRF/AVN global analysis/forecast system. *NWS Tech*. 484 (available online at <http://www.nws.noaa.gov/om/tpb/484.htm>)
- Ogasawara T, Kawamura R (2008) Effects of combined teleconnection patterns on the East Asian summer monsoon circulation: remote forcing from low-and high-latitude regions. *J Meteor Soc Jpn* 86:491–504
- Pacanowski RC, Griffies SM (1998) MOM 3.0 manual. NOAA/GFDL. (available online at [http://www.gfdl.noaa.gov/~smg/MOM/web/guide\\_parent/guide\\_parent.html](http://www.gfdl.noaa.gov/~smg/MOM/web/guide_parent/guide_parent.html))
- Park CK, Schubert S (1997) On the nature of the 1994 East Asian summer drought. *J Clim* 10:1056–1070
- Peng P, Kumar A, Barnston AG, Goddard L (2000) Simulation skills of the SST-forced global climate variability of the NCEP-MRF9 and the scripps-MPI ECHAM3 models. *J Clim* 13:3657–3679
- Rowell DP (1998) Assessing potential seasonal predictability with an ensemble of multidecadal GCM simulations. *J Clim* 11:109–120
- Saha S, Nadiga S, Thiaw C, Wang J et al (2006) The NCEP climate forecast system. *J Clim* 19:3483–3517

- Seager R, Harnik N, Kushnir Y, Robinson W, Miller J (2003) Mechanisms of hemispherically symmetric climate variability. *J Clim* 16:2960–2978
- Shukla J (1998) Predictability in the midst of chaos: a scientific basis for climate forecasting. *Science* 282:728–731
- Smith TM, Reynolds RW (2004) Improved extended reconstruction of SST (1854–1997). *J Clim* 17:2466–2477
- Wang B, An SI (2005) A method for detecting season-dependent modes of climate variability: S-EOF analysis. *GRL* 32:L15710. doi:10.1029/2005GL022709
- Wang H, Wang B (2010) Interdecadal change of the northern summer circumglobal teleconnection. Submitted to *GRL*
- Wang B, Wu R, Fu X (2000) Pacific-East Asia teleconnection: how does ENSO affect East Asian climate? *J Clim* 13:1517–1536
- Wang B, Wu RG, Lau KM (2001) Interannual variability of the Asian summer monsoon: contrasts between the Indian and the western North Pacific-east Asian monsoons. *J Clim* 14:4073–4090
- Wang B, Wu RG, Li T (2003) Atmosphere-warm ocean interaction and its impacts on Asian-Australian monsoon variation. *J Clim* 16:1195–1211
- Wang B, Lee JY, Kang IS, Shukla J, Hameed SN, Park CK (2007) Coupled predictability of seasonal tropical precipitation. *CLI-VAR Exch* 12:17–18
- Wang B, Lee JY, Kang IS, Shukla J, Park CK et al (2009) Advance and prospectus of seasonal prediction: assessment of APCC/ClipAS 14-model ensemble retrospective seasonal prediction (1980–2004). *Clim Dyn* 33:93–117
- Wu RG, Wang B (2002) A contrast of the East Asian summer monsoon-ENSO relationship between 1962–77 and 1978–93. *J Clim* 16:3742–3758
- Xie P, Arkin PA (1997) Global precipitation: a 17-year monthly analysis based on gauge observations, satellite estimates, and numerical model outputs. *Bull Am Meteor Soc* 78:2539–2558
- Xie SP, Hu K, Hafner J, Tokinaga H, Du Y, Huang G, Sampe T (2009) Indian ocean capacitor effect on Indo-western Pacific climate during the summer following El Nino. *J Clim* 22:730–747
- Zhang RH (1999) The role of Indian summer monsoon water vapor transportation on the summer rainfall anomalies in the northern part of China during the El Nino mature phase (in Chinese). *Plateau Meteor* 18:567–574
- Zhang S, Harrison MJ, Rosati A, Wittenberg A (2007) System design and evaluation of coupled ensemble data assimilation for global oceanic climate studies. *Mon Weather Rev* 135:3541–3564
- Zhang S, Rosati A, Harrison MJ, Gudgel R, Stern W (2008) GFDL's coupled ensemble data assimilation system, 1980–2006 oceanic reanalysis and its impact on ENSO forecast. Preprint for wcrp3, January 27-Feb. 2, 2008, Tokyo
- Zhong A, Hendon HH, Alves O (2005) Indian Ocean variability and its association with ENSO in a global coupled model. *J Clim* 18:3634–3649